RESEARCH ARTICLE | NOVEMBER 03 2005

Energy transfer in near-field optics

Gérard Colas des Francs; Christian Girard; Mathieu Juan; Alain Dereux

J. Chem. Phys. 123, 174709 (2005)
https://doi.org/10.1063/1.2101567

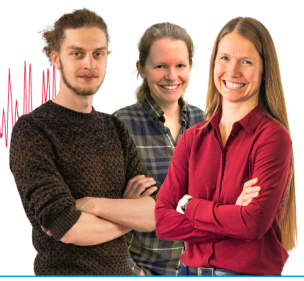

Energy transfer in near-field optics

Gérard Colas des Francs[a)]
Equipe Optique Submicronique, Laboratoire de Physique Université de Bourgogne/Centre National de la Recherche Scientifique (LPUB/CNRS), 9 Avenue Alain Savary, F-21078 Dijon, France

Christian Girard and Mathieu Juan
NanoSciences Group Centre d'Elaboration des Matériaux et d'Etudes Structurales/Centre National de la Recherche Scientifique (CEMES/CNRS), 29 rue Jeanne Marvig, BP 4347, F-31055 Toulouse, France

Alain Dereux
Equipe Optique Submicronique, Laboratoire de Physique Université de Bourgogne/Centre National de la Recherche Scientifique (LPUB/CNRS), 9 Avenue Alain Savary, F-21078 Dijon, France

(Received 15 June 2005; accepted 7 September 2005; published online 3 November 2005)

When the probe tip of a near-field optical microscope illuminates nanoparticles with marked absorption bands, a large number of photons are absorbed before reaching the detector. These energy losses enhance the dark contrast usually observed in the vicinity of metallic nanoparticles. We demonstrate theoretically that this phenomenon can be exploited to image, in the optical frequency range, dissipative domains with a nanometer scale resolution. Simulations performed with noble-metal particles indicate that the detected signal significantly drops down when the excitation frequency is approaching the plasmon resonance of the particles. © *2005 American Institute of Physics*. [DOI: 10.1063/1.2101567]

I. INTRODUCTION

Over the two last decades the extensive exploitation of all different kinds of near fields existing spontaneously or artificially at the immediate proximity of the surface of materials has generated a considerable amount of new exciting developments. Behind the average properties of these near fields (usually generated or detected by a local probe technique), it is important to emphasize that the associated particles (photons or electrons) are randomly exchanged through the gap lying between the probe tip and the surface of the material. Consequently, it becomes possible to both trigger and analyze, with a nanometer scale resolution, a large class of dissipative phenomena by controlling these different near fields.

We can first mention the scanning tunneling microscope (STM), where the introduction of some material in the gap between the source and the detector leads to well-identified dissipative phenomena. For example, tunneling electrons can be coupled to some vibration modes of the material confined inside the tunnel barrier. This gives the opportunity to perform inelastic electron tunneling spectroscopy (IETS).[1] In such experiments, the insulator embedded in the planar junction contains specified molecules. The transferred electrons are inelastically coupled to the vibration levels of these molecules.[1] We had to wait several years before the first actual experimental evidence of this effect was observed at a single molecule scale. Such observations were reported very recently[2] with C_2H_2 and C_2D_2 molecules and with CO molecules.[3]

In van der Waals force microscopy, the discrete exchange of virtual photons cannot be directly observed.[4] Although, their role could be very important in determining the noise level in the van der Waals dispersion force measurements, the virtual nature of the particles exchanged precludes a direct measure in the very near-field zone.

In near-field optics, the transfer process involves individual photonic particles as well. However, when working with standard light sources (laser) the pure quantum aspect of photon is masked by the fact that the observable electromagnetic field is an average on many photon states. With such classical waves a local density of photonic states (photonic LDOS) can be defined from Maxwell's equations.[5] In strong analogy with STM that maps the electronic LDOS of dense metallic surfaces, the scanning near-field optical microscopy (SNOM) can reveal the photonic LDOS variation sculpted by the nanostructures themselves.[6–8] Because photonic LDOS is an important parameter for the interpretation of light-matter interaction, SNOM images measuring this quantity were recorded near several systems, including semiconductor,[7,9,10] photonic crystals,[11] designed structures for light localization,[5,8,12] and plasmonic nanostructures.[13] Plasmonic nanostructures present resonant effects at visible wavelengths[14–16] generally accompanied by a significant amount of energy dissipated by Joule effect. As analyzed in the following sections, these losses can affect the imaging process in near-field optics.

Although the evanescent electromagnetic field displays imaginary wave-vector components, it may be considered as a classical quantity that will enter the coupling Hamiltonian (between electric near field and nanostructures) with the status of a parameter. Consequently, in near-field optics, a realistic description of dissipation effects is directly related to a proper description of the imaginary parts of either the dy-

[a)]Electronic mail: gerard.colas-des-francs@u-bourgogne.fr

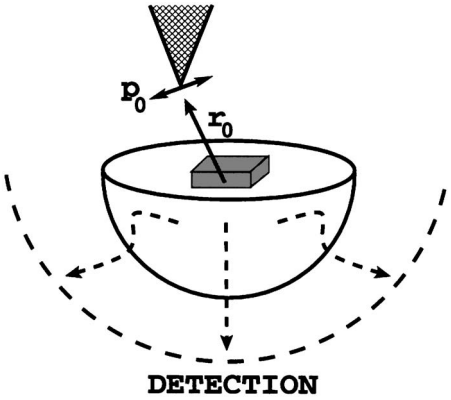

FIG. 1. Schematic representation of a SNOM setup. The active part of the probe is represented by an ideal pointlike dipolar light source $\mathbf{p}_0$ that illuminates nano-objects supported by a transparent surface. The signal transmitted below the surface is recorded in far field when the probe tip is scanned over the sample. $\mathbf{r}_0$ indicates the tip position.

namical response functions of the nanostructures or the dynamical polarizabilities of molecules adsorbed on the surface sample.

In this article, we demonstrate theoretically that the SNOM can provide a unique opportunity to image, in the optical frequency range, *dissipative regions* with a nanometer scale resolution. In particular, in the vicinity of nanoparticles with marked absorption bands, we will show that the detected signal can reveal the dissipation properties of the sample at the nanometer scale. Simulations and experiments performed with noble-metal particles indicate dramatic change of the SNOM images when working near the plasmon resonance of the particles while we observe the photon-unoccupied states maps tailored by the nanostructures when working far from these resonances.[16] As an alternative to the photothermal imaging method[17] or confocal microscopy,[18] we show how these features can be recorded with a SNOM working with a pointlike dipolar tip design.

II. SNOM SIGNAL AND ENERGY LOSSES

Figure 1 represents schematically the transmission SNOM setup considered throughout this article. A probe tip illuminates in the near-field nanostructures lithographied on a glass substrate and the energy transmitted below the surface is detected in the far-field zone with a high numerical aperture objective. Several other configurations exist. They are generally classified in two families: illuminating and collecting mode devices. The setup described in Fig. 1 belongs to the first family but, with the help of the reciprocity theorem, a strict equivalence between these two families has been demonstrated.[19] Actually, as we will see below, the main point is the high numerical aperture of the system. Therefore, SNOMs working either in collecting or emitting configuration, in which a specific direction for detection or injection is used, are not considered in this paper. Nevertheless, our formalism can be generalized to these configurations.[15,16]

In SNOM instrumentation, the optimization of local probe design can lead to efficient tips that behave like ideal emitting dipoles.[8,20–23] The signal recorded by a SNOM setup (Fig. 1) below the sample can be computed by using the Green dyadic tensor formalism.[24–26] Nevertheless, in this section, we have adopted a more pedagogical method that will enlighten on the elementary mechanisms of the energy transfer in near-field optics.[27] Furthermore, to simplify the discussion, we will assume that the intensity scattered in the whole space approximates the experimental signal usually recorded after a large detection angle below the surface.

The detected signal is then obtained in two independent steps:

(i) First, we determine the amount of light that can be emitted by the source dipole when it interacts with the sample.
(ii) In a second stage, we analyze what portion of this emitted light can really reach a far-field detector after absorption and scattering by the sample.

In the Appendix, we give a direct derivation of the signal for a simplified configuration. This leads to an original interpretation in strong analogy with the optical theorem.

A. Light emission by the probe tip

The flux of radiation emitted by a small dipolar light source is significantly modified when the dipole is brought close to an object. To introduce this basic issue, we apply the laws of electrodynamics to the geometry of Fig. 1. By applying Poynting's theorem, the power that can be delivered by the dipole source is a linear function of the current density $\mathbf{j}(\mathbf{r},t)$ associated with the fluctuating dipole (cgs units):[28]

$$I_{\text{emitted}} = -\left\langle \int_{V_0} d\mathbf{r}\mathbf{j}(\mathbf{r},t)\cdot\mathbf{E}(\mathbf{r},t)\right\rangle, \tag{1}$$

where $\mathbf{E}(\mathbf{r},t)$ defines the local electric field and V_0 is a small volume including the emitting dipole.[29] In addition, we assume that the probing dipole of magnitude p_0 oscillates according to the simple cosinusoidal law $\mathbf{p}_0(t)=\mathbf{n}p_0\cos(\omega_0 t)$ along a direction $\mathbf{n}$ located in the surface plane. The associated current density is therefore proportional to a Dirac δ function centered on the dipole position $\mathbf{r}_0$:

$$\mathbf{j}(\mathbf{r},t)=\frac{\partial\mathbf{p}_0(t)}{\partial t}\delta(\mathbf{r}-\mathbf{r}_0)=-\mathbf{n}p_0\omega_0\sin(\omega_0 t)\delta(\mathbf{r}-\mathbf{r}_0). \tag{2}$$

At this point of the demonstration, we introduce the relationship between the local electric field and its local source. That leads to a simple constitutive relation

$$\mathbf{E}(\mathbf{r},t)=\int_{-\infty}^{+\infty}dt'\mathbf{S}(\mathbf{r},\mathbf{r}_0,t-t')\cdot\mathbf{p}_0(t'), \tag{3}$$

which introduces the so-called *field-susceptibility* $\mathbf{S}(\mathbf{r},\mathbf{r}_0,t-t')$ of the optical surroundings seen by the source dipole. This dyadic tensor describes how an electric field appears in $\mathbf{r}$ when a dipole is placed in $\mathbf{r}_0$. This scattering contribution to the detected signal turns out to be proportional to the imaginary part $\text{Im}\,\mathbf{S}(\mathbf{r},\mathbf{r}_0,\omega)$ of the Fourier transform of the various components of $\mathbf{S}$. Indeed, with α and β labeling the Cartesian components x, y, and z of vectors, elementary algebra based on substituting relations (2) and (3) into Eq. (1) leads to[26]

$$I_{\text{emitted}} = -\left\langle \int_{V_0} d\mathbf{r}\mathbf{j}(\mathbf{r},t)\cdot\mathbf{E}(\mathbf{r},t)\right\rangle = \frac{\omega_0 p_0^2}{2}\sum_{\alpha,\beta} n_\alpha n_\beta \,\text{Im}\, S_{\alpha,\beta}(\mathbf{r}_0,\mathbf{r}_0,\omega_0), \tag{4}$$

where we defined the Fourier transform by ($\tau = t - t'$)

$$\mathbf{S}(\mathbf{r},\mathbf{r}_0,\omega_0) = \int_{-\infty}^{+\infty} d\tau \mathbf{S}(\mathbf{r},\mathbf{r}_0,\tau)e^{i\omega_0\tau}. \tag{5}$$

Now, to enhance the physical meaning of relation (4), it is worthwhile to introduce the concept of photonic LDOS $\rho(\mathbf{r}_0,\omega_0)$. This scalar function represents the probability to detect a photon of angular frequency ω_0 at a given position $\mathbf{r}_0$. From the scattering theory of scalar waves, it is well known that any LDOS can be formulated as a function of the imaginary part of the Fourier transform of the field susceptibility.[5,30] Here, due to the vector character of light fields, this function appears as the sum of three partial LDOS $\rho_\alpha(\mathbf{r}_0,\omega_0)$, each of them being related to each Cartesian direction

$$\rho(\mathbf{r}_0,\omega_0) = \sum_{\alpha=x,y,z} \rho_\alpha(\mathbf{r}_0,\omega_0), \tag{6}$$

where

$$\rho_\alpha(\mathbf{r}_0,\omega_0) = \frac{1}{2\pi^2\omega_0}\,\text{Im}\, S_{\alpha\alpha}(\mathbf{r}_0,\mathbf{r}_0,\omega_0). \tag{7}$$

At this point, it is instructive to fix a specific orientation α of the dipolar source $\mathbf{p}_0$ along anyone of the Cartesian axis. In this case, it is possible to establish a relation between the scattered signal and one of the partial LDOS

$$I_{\text{emitted}} = \omega_0^2\pi^2 p_0^2 \rho_\alpha(\mathbf{r}_0,\omega_0). \tag{8}$$

B. Energy dissipation into the sample

Some part of the light delivered by the source dipole is absorbed by the sample. This dissipative term[28] represents the power dissipated by the system by Joule effect. It is proportional to the imaginary part $\text{Im}[\epsilon(\mathbf{r},\omega_0)]$ of the dielectric permittivity of the nanostructures:

$$Q_{\text{diss}} = \frac{\omega_0}{8\pi}\int_{\text{object}} \text{Im}[\epsilon(\mathbf{r},\omega_0)]|\mathbf{E}(\mathbf{r},\omega_0)|^2 d\mathbf{r}, \tag{9}$$

where $\mathbf{E}(\mathbf{r},\omega_0)$ defines the local electric field inside the materials. This local field, that is directly produced by the tip, can be expressed with the field-susceptibility tensor $\mathbf{S}$ [see Eq. (3) and below].

C. Light scattered by the nanostructures

Another part of the light emitted by the dipole source is scattered by the sample. This contribution is proportional to the square modulus of the dipolar polarization $\mathbf{P}(\mathbf{r},\omega_0)$ inside the volume of the nanostructure. Indeed, each elementary volume $d\mathbf{r}$ scatters an energy:

$$\frac{\omega_0^4}{3c^3}|\mathbf{P}(\mathbf{r},\omega_0)|^2 d\mathbf{r} \tag{10}$$

per time unit, and the total power scattered by the nanostructure is given by

$$I_{\text{scatt}} = \frac{\omega_0^4}{3c^3}\int_{\text{object}} |\mathbf{P}(\mathbf{r},\omega_0)|^2 d\mathbf{r}. \tag{11}$$

In this last expression, the dipolar polarization $\mathbf{P}(\mathbf{r},\omega_0)$ is induced by the SNOM tip. Consequently, it is directly proportional to the local field $\mathbf{E}(\mathbf{r},\omega_0)$

$$\mathbf{P}(\mathbf{r},\omega_0) = \chi(\omega_0)\mathbf{E}(\mathbf{r},\omega_0) = \frac{\epsilon(\omega_0)-1}{4\pi}\mathbf{E}(\mathbf{r},\omega_0). \tag{12}$$

Let us note that expression (10) has been established from the formula of the radiative power of a dipole in vacuum. In the vicinity of a plane surface of low optical index this approximation is justified by the weakness of the LDOS variation. Furthermore, due to its induced character, contribution (11) is expected to be much weaker than the two other contributions (8) and (9) and generally appears as a small correction to the total signal.

D. Far-field detection

An expression of SNOM signal including radiative and nonradiative losses can be deduced from the previous subsections. That leads to

$$I(\mathbf{r}_0,\omega_0) = I_{\text{emitted}} + I_{\text{scatt}} - Q_{\text{diss}}, \tag{13}$$

where, with Eqs. (8), (9), and (11), we have gathered all the ingredients needed to investigate SNOM signal behavior in the presence of dissipative materials. In the following, we will discuss this problem with a single spherical nanoparticle lying at the location $\mathbf{r}_s$ on the substrate, and the emitting source dipole will be aligned along the x axis. In this case, the linear response of the nanoparticle is completely characterized by its polarizability α:

$$\chi(\mathbf{r},\omega) = \alpha(\omega)\delta(\mathbf{r}-\mathbf{r}_s) \quad \text{with } \alpha(\omega) = \alpha'(\omega) + i\alpha''(\omega). \tag{14}$$

This particle modifies the *field-susceptibility* $\mathbf{S}_0(\mathbf{r},\mathbf{r}',\omega_0)$ associated with the bare sample. At the first Born approximation, we can write

$$\mathbf{S}(\mathbf{r},\mathbf{r}',\omega_0) = \mathbf{S}_0(\mathbf{r},\mathbf{r}',\omega_0) + \mathbf{S}_0(\mathbf{r},\mathbf{r}_s,\omega_0)\cdot\alpha(\omega_0)\cdot\mathbf{S}_0(\mathbf{r}_s,\mathbf{r}',\omega_0). \tag{15}$$

Finally, after straightforward algebra, the various contributions to the signal simplify to (for the sake of clarity, we have introduced the notation $\mathbf{S}_0(\mathbf{r}_s,\mathbf{r}_0,\omega_0) = \mathbf{S}_0' + i\mathbf{S}_0''$)

$$I(\mathbf{r}_0,\omega_0) = \frac{ck_0^4 p_0^2}{3}\left[1 + \frac{|\mathbf{p_s}|^2}{|\mathbf{p}_0|^2} + \overline{\Delta\rho}_x(\mathbf{r}_0,\omega_0) - \overline{Q_{\text{diss}}}(\mathbf{r}_0,\omega_0)\right], \tag{16}$$

with

$$\mathbf{p_s} = \alpha(\omega_0)\mathbf{S}_0(\mathbf{r}_s,\mathbf{r}_0,\omega_0)\cdot\mathbf{p}_0, \tag{17}$$

$$\overline{\Delta\rho_x}(\mathbf{r}_0,\omega_0) = (\rho_x(\mathbf{r}_0,\omega_0) - \rho_x^0(\mathbf{r}_0,\omega_0))/I_0 \tag{18}$$

$$= \frac{3}{k_0^3}\alpha'(\omega_0)\sum_{\beta=x,y,z} S'_{0\beta,x}S''_{0\beta,x} + \frac{3}{2k_0^3}\alpha''(\omega_0)\sum_{\beta=x,y,z}(S'^2_{0\beta,x} - S''^2_{0\beta,x}), \tag{19}$$

and

$$\overline{Q_{\text{diss}}}(\mathbf{r}_0,\omega_0) = \frac{3}{2k_0^3}\alpha''(\omega_0)\sum_{\beta=x,y,z}(S'^2_{0\beta,x} + S''^2_{0\beta,x}). \tag{20}$$

The overline indicates that the parameter is normalized with respect to the free-space signal $I_0 = ck_0^4p_0^2/3$ ($k_0 = \omega_0/c$). The physical meaning of expression (16) appears clearly:

(i) the first two terms represent the scattering of both source $\mathbf{p}_0$ and induced dipoles $\mathbf{p}_\mathbf{s}$, respectively.
(ii) the x-LDOS $\overline{\Delta\rho_x}$ variation describes how the nanoparticle modifies the emission process of the source dipole.
(iii) the last term accounts for the energy dissipation inside the nanoparticle.

Let us remember that this expression is not rigorously exact because the induced dipole scattering term includes an approximation [cf. previous remark concerning Eq. (11)]. However, it compares rigorously with the direct calculation exposed in the Appendix where we have removed the bearing surface. For more complex geometry, the emitted and the dissipative contributions to the signal are treated exactly in Eq. (16). Finally, a detailed comparison between the different terms of expressions (19) and (20) shows that a part of photons emitted by the tip dipole is then immediately reabsorbed by the particle (term $3/2k_0^3\alpha''(\omega_0)\Sigma S'^2_{0\beta,x}$). After combining the different relations [(16)–(20)], the SNOM signal reduces to

$$I(\mathbf{r}_0,\omega_0) = \frac{ck_0^4p_0^2}{3}\left\{1 + |\alpha(\omega_0)|^2\sum_{\beta=x,y,z} S''^2_{0\beta,x} + \frac{3}{k_0^3}\left[\alpha'(\omega_0)\sum_{\beta=x,y,z} S'_{0\beta,x}S''_{0\beta,x} - \alpha''(\omega_0)\sum_{\beta=x,y,z} S''^2_{0\beta,x}\right]\right\}. \tag{21}$$

This last expression is reminiscent from the *inelastic tunneling current* measured and described in Ref. 31. It shows precisely the balance between scattering and dissipation when the nanoparticle is locally excited [see also relation (A6) in the Appendix]. Apart from the scattered part (term in $|\alpha|^2$), the major contribution of the signal depends on the third power of the particle radius a. It is of great interest for optical characterization of very small particles. Similar expression has been derivated for confocal microscopy.[18]

III. NUMERICAL RESULTS

From the dielectric data of Ref. 32, we have applied our formalism to a single silver particle (cf. Fig. 2). In the vicinity of $\omega_0 = \omega_p = 3.2$ eV, the dipolar polarizability is greatly enhanced revealing the excitation of a localized plasmon mode. As expected, this resonance corresponds to a sign change of the real part of the polarizability. Far away from this resonance, we have plotted in Fig. 3(a) the individual variations of the LDOS [Eq. (19)], dissipative [Eq. (20)], and induced dipole scattering [Eq. (17)] contributions to the total signal. In this off-resonance regime, we note that the main contribution to the signal is produced by the lateral variation

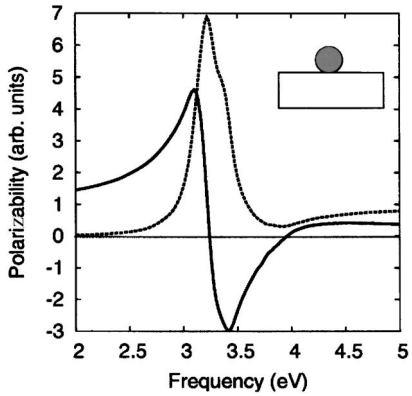

FIG. 2. Numerical simulation performed with a single silver particle [including the surface coupling (Ref. 24)]. Plot of the spectral variation of the dipolar polarizability (solid line: real part, dashed line: imaginary part).

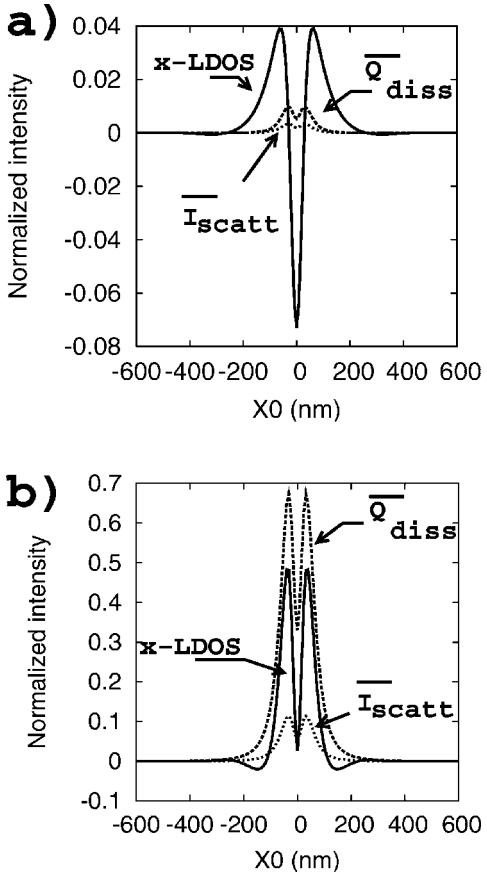

FIG. 3. Numerical simulation of the contributions to the total signal detected when a dipole is scanned over a single silver nanoparticle supported by a transparent surface. (a) Off-resonant wavelength ($\omega_0 = 2$ eV). (b) Resonant wavelength ($\omega_0 = 3.2$ eV). All the signals are normalized with respect to their value without the silver particle.

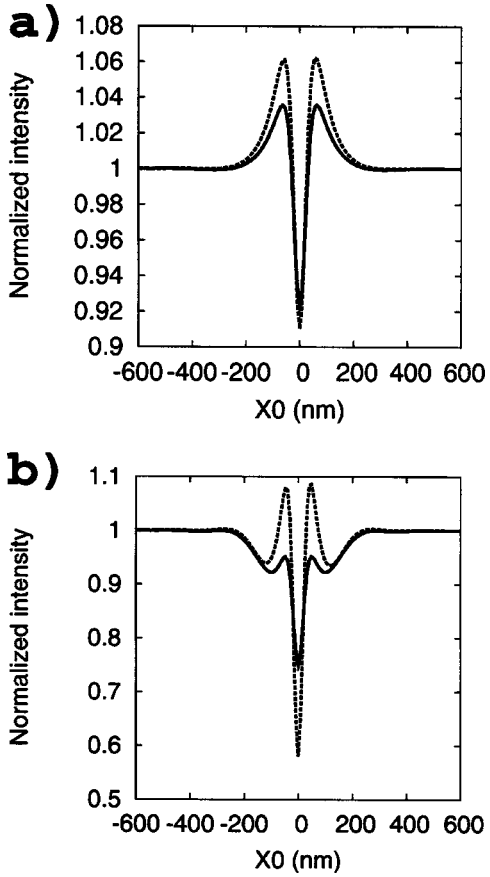

FIG. 4. Direct numerical integration of the signal transmitted below the surface (dashed curve) and signal obtained from the approximated expression (21) (solid curve) at $\omega_0=2$ eV (c) and $\omega_0=3.2$ eV (d). All the signals are normalized with respect to their value without the silver particle.

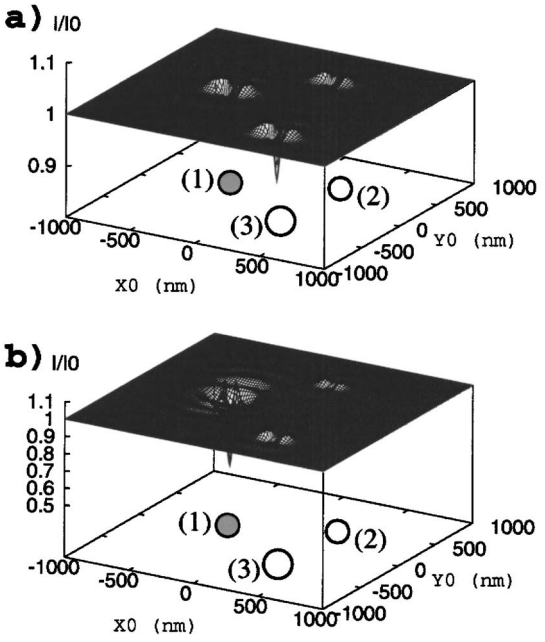

FIG. 5. SNOM images computed in the vicinity of nanometer-sized metal particles among dielectric scatterers. The tip dipole is oriented along the x axis and scans the sample at a constant distance $Z_d=80$ nm from the surface. (1) is a 20-nm-radius silver nanoparticle, while (2) and (3) designate, respectively, two 20-nm-radius and 25-nm-radius dielectric particles (optical index of 2.2). (a) frequency $\omega_0=2$ eV and (b) $\omega_0=3.2$ eV. The calculated signal is obtained by the numerical integration of the signal transmitted below the surface.

of the x-LDOS. Both induced scattering and dissipative contributions remain weak. Recently, SNOM experimental signals have been recorded near both metal particles[8] and metallic patterned structures[21] by working far from any localized resonances. These data display similar contrast reversal when the tip scans above the structures.

Let us see what happens when the excitation frequency comes closer and closer to ω_p [see Figs. 3(b) and 4(b)]. According to the polarizability variations, we observe a neat enhancement of the so-called *dissipative signal*. As discussed above, a large amount of photons does not reach the detector because of the absorption process (Q_{diss}). Consequently, this effect tends to reinforce and enlarge the depression of the scan line around the metal particle. In conclusion, an increasing of the dark contrast areas is associated with some absorption phenomena [Fig. 4(b)].[13,33]

We have also computed the SNOM signal by applying a numerical integration of the electric intensity transmitted below the surface (see Ref. 26 for details). Far from the resonance, the analytical expression (21) reproduces satisfactorily the exact calculation [Fig. 4(a)]. These two numerical simulations reveal that the small difference is not related to the evaluation of the scattered contribution in (21), but it rather originates from the 4π sr solid angle integration used to obtain the analytical expression (21).[34] At the plasmon resonance, the divergence between analytical and numerical approaches increases [Fig. 4(b)]. Nevertheless, even in this particular case, our analytical expression remains precious for the understanding of elementary mechanisms of the energy transport from probe tips towards detectors.

To get more insight on the transition between scattering and dissipation regimes, we have simulated in Fig. 5 two SNOM images with a single nanometer scale Ag particle located among two other optically inactive particles of different sizes. Far away from the plasmon resonance, the Ag particle [labeled (1)] behaves like the two other ones with the usual image shape that is associated with a polarized x-LDOS change.[8,26] Near the resonance frequency of the silver particle, the image displays profound changes. The dark contrast observed around the silver particle increases dramatically and tends to weaken the visibility of the other nondissipative particles. In this case, the SNOM maps look different from the usual partial LDOS maps observed in the off-resonance regime.

IV. CONCLUSION

To conclude, we have presented calculations of the influence of dissipation effects on the SNOM image formation. We have shown that the position of the excitation frequency with respect to the resonance frequencies of the object can lead to drastic changes of the expected contrast. The results are in overall good agreement with previous experiments performed in the off-resonant regime in the vicinity of metallic posts and could be a useful guide to extract the dissi-

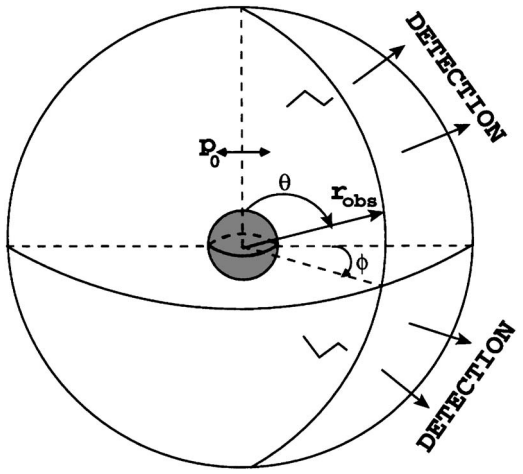

FIG. 6. Configuration used for a direct calculation of the SNOM signal. An ideal pointlike dipolar light source illuminates a nanoparticle. The scattered light is collected in the whole space.

pation map from SNOM signal near the resonance. This could also be an interesting alternative to the photothermal imaging method described recently.[17,35]

ACKNOWLEDGMENTS

The cooperation of the authors profits from the European Network of Excellence (NoE) Plasmo-Nano-Devices (Contract No. FP6 2002-IST-1-507879) and the Specific Target Research Project (STRP) ASPRINT (Contract No. NMP-CT-2003-001601) in the sixth Framework Program of the European Community.

APPENDIX: DIRECT CALCULATION OF THE SNOM SIGNAL

When considering the simple configuration of Fig. 6, from the first principles of electrodynamics, one can elaborate a rigorous analytical expression of the scattered signal without splitting the total power in three parts (emitted, scattered, and absorbed). This second approach will be used to compare with the results obtained in Sec. II.

The dipole source is moved in front of a spherical nanoparticle of radius a, located at $\mathbf{r}_s=(0,0,0)$. For simplicity, we restrict our demonstration to a dipole source aligned along the x axis $\mathbf{p}_0=p_0\mathbf{e}_x$ and moving vertically $[\mathbf{r}_0=(0,0,z_0)]$. The complete demonstration can easily be generalized to arbitrary configuration.

The ω-Fourier transform of the fluctuating dipole $\mathbf{p}_s(\omega)$ induced in the particle by the source dipole $\mathbf{p}_0(\omega)$ is proportional to the dipolar polarizability $\alpha(\omega)$ of the particle. One has then

$$\mathbf{p}_s(\omega)=\alpha(\omega)\mathbf{E}(\mathbf{r}_s,\omega)=\alpha(\omega_0)\left[\frac{k_0^2}{z_0}+i\frac{k_0}{z_0^2}-\frac{1}{z_0^3}\right]e^{ik_0z_0}p_0\mathbf{e}_x. \tag{A1}$$

The electric field emitted by these two dipoles at a point $\mathbf{r}_{obs}$ located in the far-field zone is given by

$$\mathbf{E}(\mathbf{r}_{obs},\omega)=\mathbf{S}_\infty(\mathbf{r}_{obs},\mathbf{r}_0,\omega)\cdot\mathbf{p}_0+\mathbf{S}_\infty(\mathbf{r}_{obs},\mathbf{r}_s,\omega)\cdot\mathbf{p}_s, \tag{A2}$$

where

$$\begin{aligned}\mathbf{S}_\infty(\mathbf{r}_{obs},\mathbf{r}_i,\omega)\cdot\mathbf{e}_x=k_0^2\frac{e^{ik_0r_{obs}}}{r_{obs}}e^{ik_0z_i\cos\theta}&\\ \times[1-\sin^2\theta\cos^2\phi)\mathbf{e}_x&\\ -\sin^2\theta\cos\phi\sin\phi\mathbf{e}_y&\\ -\sin\theta\cos\theta\cos\phi\mathbf{e}_z]&\end{aligned} \tag{A3}$$

is the field radiated by a unit dipole oriented along the x axis. r_{obs}, θ, and ϕ are the three spherical coordinates used to locate the observation point. If one assumes an energy collection over a solid angle of 4π sr, the recorded signal is

$$I(z_0)=\frac{c}{8\pi}\int_0^\pi d\theta\int_0^{2\pi}d\phi\mathbf{r}_{obs}^2|\mathbf{E}(\mathbf{r}_{obs},\omega)|^2\sin\theta. \tag{A4}$$

After introducing expression (A2) in this equation, we can distinguish several contributions to the signal:

$$\begin{aligned}I(z_0)=\frac{ck_0^4p_0^2}{8\pi}\int_0^\pi d\theta\int_0^{2\pi}d\phi[1+|\alpha(\omega_0)|^2|s_1|^2&\\ +2\alpha'(\omega_0)\mathrm{Re}(s_1e^{ik_0z_0\cos\theta})&\\ -2\alpha''(\omega_0)\mathrm{Im}(s_1e^{ik_0z_0\cos\theta})](1-\sin^2\theta\cos^2\phi)&\end{aligned} \tag{A5}$$

with $s_1=[(k_0^2/z_0)+i(k_0/z_0^2)-(1/z_0^3)]e^{ik_0z_0}$. After evaluation of the angular integrals, we obtain

$$\begin{aligned}I(z_0)=\frac{ck_0^4p_0^2}{3}\Bigg[1+|\alpha(\omega_0)|^2\left(\frac{1}{z_0^6}-\frac{k_0^2}{z_0^4}+\frac{k_0^4}{z_0^2}\right)&\\ +\frac{3}{2}\alpha'(\omega_0)\sin(2k_0z_0)\left(\frac{k_0}{z_0^2}-\frac{3}{k_0z_0^4}+\frac{1}{k_0^3z_0^6}\right)&\\ +\frac{3}{2}\alpha'(\omega_0)\cos(2k_0z_0)\left(\frac{2}{z_0^3}-\frac{2}{k_0^2z_0^5}\right)&\\ -\frac{3}{2}\alpha''(\omega_0)\sin(2k_0z_0)\left(\frac{2}{z_0^3}-\frac{2}{k_0^2z_0^5}\right)&\\ -\frac{3}{2}\alpha''(\omega_0)\cos(2k_0z_0)\left(\frac{3}{k_0z_0^4}-\frac{k_0^2}{z_0^2}-\frac{1}{k_0^3z_0^6}\right)&\\ -\frac{3}{2}\alpha''(\omega_0)\left(\frac{1}{k_0^3z_0^6}-\frac{1}{k_0z_0^4}+\frac{k_0}{z_0^2}\right)\Bigg].&\end{aligned} \tag{A6}$$

The physical meaning of the first and last lines of this expression is straightforward using relation (A1).

- The first term is the signal scattered by the dipole source.
- The second term can be rewritten in the form $|\alpha(\omega_0)|^2(1/z_0^6-k_0^2/z_0^4+k_0^4/z_0^2)=|\mathbf{p}_s|^2/|\mathbf{p}_0|^2$ so that it clearly represents the induced dipole scattering.
- Similarly, the last term is rewritten as $3/2\alpha''(\omega_0)\times(1/k_0^3z_0^6-1/k_0z_0^4+k_0/z_0^2)]=3/2k_0^3\alpha''(\omega_0)|\mathbf{E}(\mathbf{r}_s)|^2/|\mathbf{p}_0|^2$ which is the energy dissipated inside the nanoparticle [see Eq. (9)].

The other terms describe an interferential term between the light emitted by the source and induced dipole. Finally, after introducing the vacuum field-susceptibility expression in relation (21), we recover the result (A6) of this Appendix. In strong analogy with the *optical theorem*,[28,36] the interferences between the light emitted directly by the dipole source and the light scattered by the nanoparticle are responsible for the source emission modification described by the LDOS [see Eq. (8)].

[1] P. K. Hansma, *Tunneling Spectroscopy* (Plenum, New York, 1982).
[2] B. Stipe, M. Rezaei, and W. Ho, Science **279**, 1907 (1998).
[3] L. Lauhon and W. Ho, Phys. Rev. B **60**, R8525 (1999).
[4] U. Hartmann, Phys. Rev. B **42**, 1541 (1990).
[5] P. de Vries, D. V. van Coeverden, and A. Lagendijk, Rev. Mod. Phys. **70**, 447 (1998).
[6] R. Carminati and J. J. Sáenz, Phys. Rev. Lett. **84**, 5156 (2000).
[7] J. Guest, T. Stievater, G. Chen, E. Tabak, B. Orr, D. Steel, D. Gammon, and D. Katzer, Science **293**, 2224 (2001).
[8] C. Chicanne, T. David, R. Quidant, J. C. Weeber, Y. Lacroute, E. Bourillot, A. Dereux, G. Colas des Francs, and C. Girard, Phys. Rev. Lett. **88**, 097402 (2002).
[9] K. Matsuda, T. Saiki, S. Nomura, M. Mihara, Y. Aoyagi, S. Nair, and T. Takagahara, Phys. Rev. Lett. **91**, 177401 (2003).
[10] O. D. Stefano, S. Savasta, G. Pistone, G. Martino, and R. Girlanda, Phys. Rev. B **68**, 165329 (2003).
[11] E. Flück, N. van Hulst, W. Vos, and L. Kuipers, Phys. Rev. E **68**, 015601(R) (2003).
[12] C. Girard, T. David, C. Chicanne, A. Mary, G. Colas des Francs, E. Bourillot, J. Weeber, and A. Dereux, Europhys. Lett. **68**, 797 (2004).
[13] K. Imura, T. Nagahara, and H. Okamoto, J. Chem. Phys. **122**, 154701 (2005).
[14] J. P. Kottmann, O. J. F. Martin, D. R. Smith, and S. Schultz, Phys. Rev. B **64**, 235402 (2001).
[15] G. Wurtz, J. Hranisavljevic, and G. Wiederrecht, Nano Lett. **3**, 1511 (2003).
[16] G. Wiederrecht, Eur. Phys. J.: Appl. Phys. **28**, 3 (2004).
[17] D. Boyer, P. Tamarat, A. Maali, M. Orrit, and B. Lounis, Science **297**, 1160 (2002).
[18] K. Lindfors, T. Kalkbrenner, P. Stoller, and V. Sandoghdar, Phys. Rev. Lett. **93**, 037401 (2004).
[19] E. R. Méndez, J.-J. Greffet, and R. Carminati, Opt. Commun. **142**, 7 (1997).
[20] K. Lieberman, S. Harush, A. Lewis, and R. Kopelman, Science **247**, 59 (1990).
[21] J. Michaelis, J. M. C. Hettich, and V. Sandogdhar, Nature (London) **405**, 325 (2000).
[22] U. C. Fischer, A. Dereux, and J. C. Weeber, in *Near Field Optics and Surface Plasmon Polaritons*, edited by S. Kawata (Springer, Berlin, 2001), chap. 4, pp. 49–69.
[23] N. Chevalier, M. J. Nasse, J. C. Woehl, P. Reiss, J. Bleuse, F. Chandezon, and S. Huant, Nanotechnology **16**, 613 (2005).
[24] H. Metiu, Prog. Surf. Sci. **17**, 153 (1984).
[25] L. Novotny, J. Opt. Soc. Am. A **14**, 105 (1997).
[26] G. Colas des Francs, C. Girard, and A. Dereux, J. Chem. Phys. **117**, 4659 (2002).
[27] P. Das and H. Metiu, J. Phys. Chem. **89**, 4680 (1985).
[28] J. Jackson, *Classical Electrodynamics*, 3rd ed. (Wiley, Hoboken, 1998).
[29] In previous papers, we consider a volume large enough to include the sample, this leads to neglect both the scattering and dissipation by the sample term, approximation which is no more valuable here; see also S. Savasta, O. D. Stefano, R. Girlanda, and M. Pieruccini, Phys. Rev. Lett. **93**, 069701 (2004); C. Chicanne, T. David, R. Quidant, J. C. Weeber, Y. Lacroute, E. Bourillot, A. Dereux, G. Colas des Francs, and C. Gerard, *ibid.* **93**, 069702 (2004).
[30] E. N. Economou, *Green's Functions in Quantum Physics*, Springer Series in Solid-State Science, Vol. 7, 2nd ed. (Springer, Berlin, 1983).
[31] N. Lorente and M. Persson, Phys. Rev. Lett. **85**, 2997 (2000).
[32] Z. Palik, *Handbook of Optical Constants of Solids* (Academic, San Diego, CA, 1985).
[33] C. Hubert, A. Rumyantseva, G. Lerondel *et al.*, Nano Lett. **5**, 615 (2005).
[34] G. Colas des Francs, C. Girard, J. C. Weeber, and A. Dereux, Chem. Phys. Lett. **345**, 512 (2001).
[35] A. Arbouet, D. Christofilos, N. D. Fatti, F. Valle, J. R. Huntzinger, L. Arnaud, P. Billaud, and M. Broyer, Phys. Rev. Lett. **93**, 127401 (2004).
[36] H. van de Hulst, *Light Scattering by Small Particles*, 1st ed. (Dover, New York, 1981).